

Towards the Training of Deeper Predictive Coding Neural Networks

Chang Qi¹, Matteo Forasassi¹, Thomas Lukasiewicz^{1,2}, Tommaso Salvatori^{3,1}

¹Institute of Logic and Computation, Vienna University of Technology, Vienna, Austria

²University of Oxford, UK ³VERSES AI Research Lab, Los Angeles, US

chang.qi@tuwien.ac.at, matteo.forasassi@tuwien.ac.at,

thomas.lukasiewicz@tuwien.ac.at, tommaso.salvatori@verses.ai

Abstract

Predictive coding networks trained with equilibrium propagation are neural models that perform inference through an iterative energy minimization process. Previous studies have demonstrated their effectiveness in shallow architectures, but show significant performance degradation when depth exceeds five to seven layers. In this work, we show that the reason behind this degradation is due to exponentially imbalanced errors between layers during weight updates, and predictions from the previous layer not being effective in guiding updates in deeper layers. We address the first issue by introducing two novel methods to optimize the latent variables that use precision-weighting to re-balance the distribution of energy among layers during the ‘relaxation phase’, and the second issue by proposing a novel weight update mechanism that reduces error accumulation in deeper layers. Empirically, we test our methods on a large number of image classification tasks, resulting in large improvements in test accuracy across networks with more than seven layers, with performances comparable to those of backprop on similar models. These findings suggest that a better understanding of the relaxation phase is important to train models using equilibrium propagation at scale, and open new possibilities for their application in complex tasks.

1 Introduction

Training large-scale models on GPUs is extremely expensive in terms of energy consumption. To address this problem, a recent direction of research is studying the use of alternative accelerators that leverage the properties of physical systems to perform computations [Wright et al., 2022, Momeni et al., 2024]. A popular example is hardware that performs in-memory computations using memristor crossbars [Tsai et al., 2018, Haensch et al., 2018]. However, transitioning to new hardware without altering the main algorithm — error backpropagation [Rumelhart et al., 1986] — has proven to be challenging due to two central issues: the requirement of sequential forward and backward passes, and the need to analytically compute gradients of a global cost function. These requirements necessitate digital hardware architectures that precisely match forward computations with their corresponding gradient calculations in low-noise environments, as even minor fluctuations can propagate numerical errors that can alter the final performance of the model.

To address the above problems, there is a direction of research that has studied learning algorithms for deep neural networks that rely on local computations only [Bengio, 2014, Hinton, 2022]. One way of doing this is by training the model using equilibrium propagation, a framework that allows the learning of the parameters of a neural network by simulating a physical system brought to an equilibrium [Scellier and Bengio, 2017]. This physical system is usually defined via an energy function that describes the state of a neural network in terms of its weights and neurons, with different functions describing different systems [Hopfield, 1982, Krotov and Hopfield, 2016].

In recent years, researchers have devoted significant effort to scaling up the deployment of energy-based models. Two recent works have also carefully benchmarked multiple variations of the usual learning algorithms by using the Hopfield energy function [Scellier et al., 2024], and the predictive coding energy [Pinchetti et al., 2024], showing that this class of models is able to perform as well as standard deep learning models trained with backpropagation when it comes to training shallow models, with a maximum of five or seven layers. This result, however, does not translate to the case of deeper models, where we observe a significant degradation of performance. As most of the successes of modern deep learning rely on very deep architectures, understanding and addressing the causes of this degradation is then of vital importance if we aim to train large-scale predictive coding networks.

It has recently been shown that in a three-layer model, the energy concentrated in a layer can be up to an order of magnitude larger than the energy concentrated in the layer before [Pinchetti et al., 2024]. While such shallow models can still achieve good test accuracies, we conjecture that this ‘energy imbalance’ becomes a critical bottleneck in deeper architectures, leading to performance degradation in a way that is conceptually similar to the *vanishing gradient* problem [Hochreiter, 1998]. More precisely, this imbalance prevents the effective propagation of energy — and crucially, the associated error information — from the output layer back to the early layers, creating two problems: first, it prevents the model from fully leveraging its depth, as early layers receive insufficient error signals for effective training; second, latent states may diverge substantially from their forward pass values, due to the excessive energy in later layers, thereby resulting in sub-optimal weight updates.

Addressing this energy imbalance requires mechanisms that can adaptively modulate the energy of different layers as it propagates through the network — a challenge remarkably similar to what biological neural systems solve through precision-based regulation [Clark, 2013, Mumford, 1992]. In the brain, the flow of information is in fact believed to be heavily influenced by *precision weighting*, a mechanism that dynamically rescales error terms, effectively balancing top-down and bottom-up signals between different brain regions [Rao and Ballard, 1999, Friston, 2005, Friston and Kiebel, 2009, Clark, 2013]. Despite its central role in biological systems, precision weighting has been largely overlooked in machine learning applications, and often set to 1 in experimental setups when considered in algorithmic descriptions [Whittington and Bogacz, 2017, Salvatori et al., 2023, Song et al., 2020]. Inspired by this neuroscientific principle, we propose to leverage precisions to regularize energy propagation in predictive coding networks, aiming to improve their performance in image classification tasks by addressing the identified energy imbalance. We do so by first analyzing the energy propagation of deep convolutional architectures, and then propose time-dependent precisions that address them. The results show that this largely improves test accuracies, hence confirming our conjecture of a causal relation between energy propagation and empirical results. Our contributions are briefly as follows:

- We empirically study the propagation of the energy on different layers of the model, and show that such energy is orders of magnitudes larger in the layers closer to the label, and almost non existent in the first layers. This strongly supports the hypothesis that the energy of deep models fail to reach the first layers. We also show that a similar phenomenon is not observed in high-performing models trained with backpropagation.
- To address this imbalance, and test on whether it impacts the final test accuracy of the model, we propose two different combinations of precision-weighting, which depend on both time and layer number. The first proposal, called *spiking precision* leverages very large precisions as soon as the energy reaches a specific layer, to boost it towards the following layer. The second proposal, which we call *decaying precision*, introduces an exponential decay in precisions that heavily penalize later layers. The results show that both methods regulate the energy imbalance, with the spiking precision providing the largest improvements in terms of test accuracies in deep models. In addition, we also propose a variation of batch normalization [Ioffe and Szegedy, 2015], which further improves the results under the novel kinds of inference.
- To further boost the results, we introduce a novel weight update mechanism that changes the way weight parameters are updated. This method uses both the predictions computed at initializations (hence adding a degree of implausibility), and the neural activities at convergence, to compute the updates. Again, the results show that this largely improves the performance of predictive coding networks in models with more than ten layers. Furthermore, combining our novel weight updates and precision-weighted inference allows us to reach competitive results against backprop on challenging benchmarks for the biologically-plausible community, such as the training of convolutional models with 15 layers on Tiny ImageNet.

2 Related Works

Equilibrium Propagation (EP). EP is a learning algorithm for supervised learning that is largely inspired by contrastive learning on continuous Hopfield networks [Movellan, 1991]. Here, neural activities are updated in two phases: In the first, to minimize an energy function defined on the parameters of the neural network; in the second, to minimize the same energy with the addition of a loss function defined on the labels [Scellier and Bengio, 2017]. Interestingly, these two phases allow us to approximate the gradient of the loss function up to arbitrary levels of accuracy using finite difference coefficients [Zucchet and Sacramento, 2022]. The consequence is that EP can be seen as a technique that allows the minimization of loss functions using arbitrary physical systems that can be brought to an equilibrium, and it has hence been studied in a large number of domains [Scellier, 2024, Kendall et al., 2020]. In terms of simulations that aim to scale up machine learning experiments, most of the works performed experiments using Hopfield energies [Hopfield, 1982], mostly on image classification tasks using convolutional networks [Laborieux et al., 2021, Laborieux and Zenke, 2022]. The state of the art is that EP models are able to match the performance of BPTT (BP Through Time) on models with 5 and 7 hidden layers [Scellier et al., 2024], with the exception of hybrid models, which manage to achieve a good performance on models with 15 layers by alternating blocks of layers trained with BP and blocks trained with EP [Nest and Ernault, 2024].

Predictive Coding (PC). The formulation of PC that we use here was initially developed to model hierarchical information processing in the brain [Rao and Ballard, 1999, Friston, 2005]. Intuitively, this theory states that neurons and synapses at one level of the hierarchy are updated to better predict the activities of the neurons of the layers below, and hence minimize the *prediction error*. Interestingly, the same algorithm can be used as a training algorithm for deep neural networks [Whittington and Bogacz, 2017], where several similarities with backpropagation were observed [Song et al., 2020, Salvatori et al., 2022a]. To this end, it has been used in a large number of machine learning tasks, from image generation and classification to natural language processing and associative memory [Sennesh et al., 2024, Salvatori et al., 2023, Pinchetti et al., 2022, Ororbia and Kifer, 2020, Salvatori et al., 2021]. Again, the state of the art has been reached by training convolutional models with 5 hidden layers, with performance starting to get worse as soon as we use models that are 7 layers deep [Pinchetti et al., 2024]. The connection between PC and EP is well explained by the concept of bi-level optimization [Zucchet and Sacramento, 2022], where the neural activities used for learning are the equilibrium state of a physical system. For a description of a more general framework that describes learning in this setup but is agnostic to the physical system and energy function used, we refer to two recent works [Ernault et al., Scellier et al., 2022].

3 Background

Let us consider a neural network with L layers, and let us denote \mathbf{W}^l and \mathbf{x}_t^l the weight parameters and the neural activities of layer l , respectively. Note that, differently from standard models trained with BP, the neural activities are variables of the model, optimized over multiple time steps t . This optimization is performed with the goal of allowing the activities of every layer to predict those of the layer below. Together with the neural activities, the two other quantities usually related to single neurons are the *prediction* $\mu_t^l = \mathbf{W}^l \mathbf{f}(\mathbf{x}_t^{l-1})$, given by the layer-wise operation through an activation function, and the *prediction error*, defined as the deviation of the actual activity from the prediction, that is, $\epsilon_t^l = \mathbf{x}_t^l - \mu_t^l$. A fourth quantity, usually overlooked in machine learning applications but of vital importance in neuroscience, is the *precision*, or *covariance* Σ_t^l of a specific neuron ¹. Differently from the standard literature, however, we consider the covariance to be time-dependent. Furthermore, instead of updating it to minimize an objective function as done in previous works Ofner et al. [2021], we will manually define the rule that governs its updates. The predictive coding energy is then the sum of the squared norms of the precision-weighted prediction errors of every layer over time:

$$E_t = \frac{1}{2} \sum_{l=1}^L \frac{\|\mathbf{x}_t^l - \mu_t^l\|^2}{\Sigma_t^l} = \frac{1}{2} \sum_{l=1}^L \frac{\|\epsilon_t^l\|^2}{\Sigma_t^l}, \quad (1)$$

¹In predictive coding, and more generally in statistics, the precision matrix is the matrix inverse of the covariance matrix. In this work, we follow the standard convention and divide the prediction error by a factor of Σ , instead of multiplying it by a factor of p .

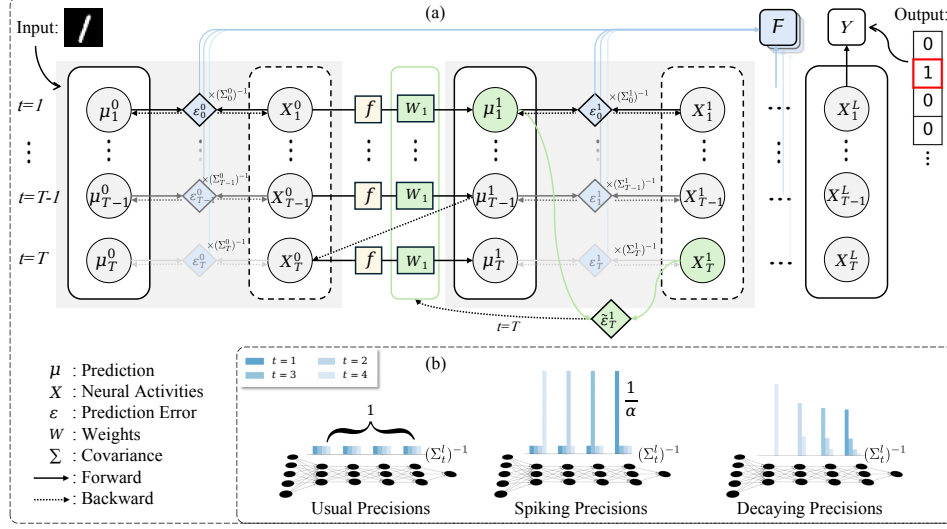


Figure 1: (a) Evolution of predictive coding models over multiple time iterations. The green diamond ε_T^{l+1} refers to the information needed to compute the proposed forward updates. The rest of the figure represents the standard components and mechanisms of a predictive coding network. (b) Visualization of the proposed precision-weighting strategies, where the height of the bar is proportional to the precision at different time steps.

where we consider covariances to be layer-dependent: all the neurons of the same layer will have the same covariance. To this end, we use the same notation when the covariance Σ_t^l is a scalar value, or a diagonal matrix whose entries are equal to such a scalar. For a detailed representation of a predictive coding network, we refer to Figure 1(a).

Training. Suppose that we are provided with a labeled data point (\mathbf{o}, \mathbf{y}) , where \mathbf{o} denotes sensory inputs, and $\mathbf{y} \in \mathbb{R}^o$ is the label. Training is then performed via a form of bi-level optimization [Zucchet and Sacramento, 2022], divided into three phases. In the first phase, the neural activities of every neuron are initialized via a forward pass, that is, we set $\mathbf{x}_0^1 = \mu_0^1$ for every layer, with $x_0^0 = o$. In the second phase, that we call the *inference* phase, we fix the neural activities of the output layer to the label, that is, we set $\mathbf{x}_L = \mathbf{y}$, and we update the neural activities via gradient descent, to minimize the total energy of the model. The update rule is then the following:

$$\Delta \mathbf{x}_t^l = -\alpha \frac{\partial E_t}{\partial \mathbf{x}_t^l} = \alpha \left(\frac{\varepsilon_t^l}{\Sigma_t^l} - \mathbf{W}^{(l+1)\top} \frac{\varepsilon_t^{l+1}}{\Sigma_t^l} \odot f'(\mathbf{x}_t^l) \right), \quad (2)$$

where α is the learning rate of the neural activities. This phase will continue until it reaches the fixed number of iterations \mathbf{T} or achieves convergence. The third phase is the *learning* phase, where the neural activities \mathbf{x}_T^l are fixed, and the weight parameters are updated to decrease the energy, weighted by a learning rate η , via the following equation:

$$\Delta \mathbf{W}^l = -\eta \frac{\partial E_T}{\partial \mathbf{W}^l} = -\eta \frac{\varepsilon_T^l f(\mathbf{x}_T^{l-1})}{\Sigma_T^l}, \quad (3)$$

Nudging as Precision. Instead of providing the original label y to the model, it is common in the literature to slightly translate the output neurons of the system \mathbf{x}_0^L in the direction of y . More precisely, it fixes $\mathbf{x}_t^L = \mu_0^L + \beta(\mathbf{y} - \mu_0^L)$ for every time step t , where β controls the supervision strength. The sign of β determines supervision polarity: positive for standard nudging and negative for inverse supervision. Performing a stochastic sampling from $\{\beta, -\beta\}$ across training epochs and batches is called *center nudging* [Scellier et al., 2024]. In practice, the term β scales the prediction error at the output layer, meaning that it functions as the "gain" or "precision" with which the error signal influences the state of the model, effectively controlling the strength and direction of the information flow from the desired output back into the system, much like precision weighting alters error unit gain and balances signals in predictive coding. To this end, it is possible to describe the same phenomenon using standard predictive coding and our dynamical precision weighting by simply setting $(\Sigma_t^L)^{-1} = \beta$ for every t .

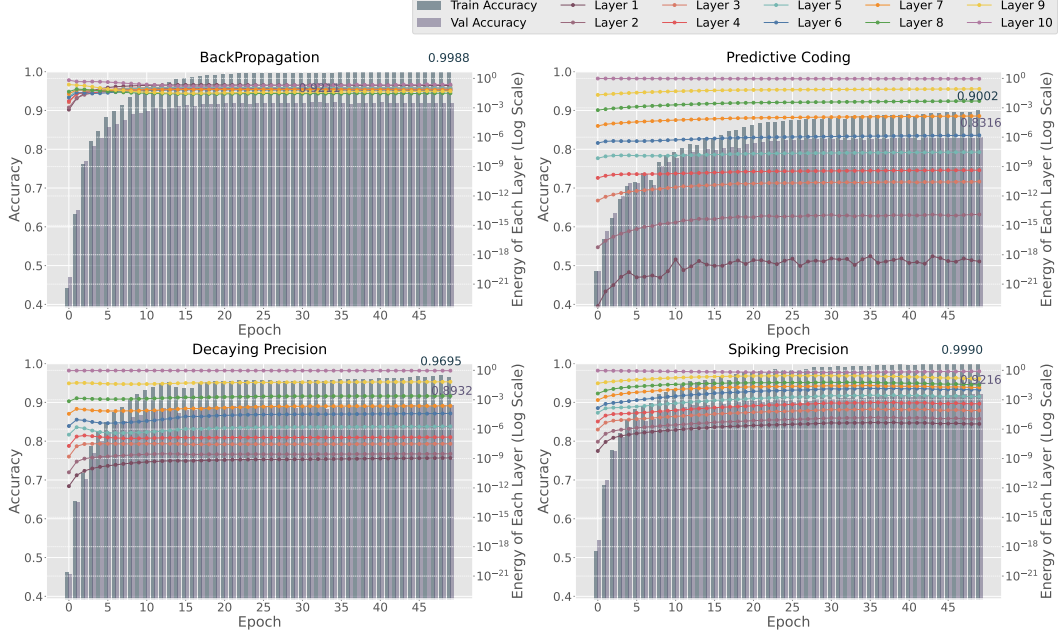


Figure 2: Layer-wise energy distribution and accuracy comparison between BP and PCNs in a VGG10 on the CIFAR10 dataset. Colored curves represent the total energy of the individual layers of the model (or, the squared error of every layer for BP). The vertical lines represent the train and test accuracies of the model.

4 Methods

In this section, we first study the phenomenon of energy imbalance across different layers, and then use the derived insights to define different formulations of time-dependent covariances that address it. In detail, we introduce two methods, called *spiking precisions* and *decaying precisions*, each offering distinct strategies to better distribute the energy across the model by dynamically updating the precisions. We also introduce a variation of the learning phase, which leverages neural activities at initialization to perform a better update of the parameters and improve overall model performance. We conclude with a novel formulation of the batch normalization, more suitable to the training of PCNs. We will show that this novel formulation will not have a large impact in terms of performance when used in combination with the standard formulation of PC. However, it will result in a large gain when tested with our newly proposed methods. To facilitate a better understanding of our proposed algorithms, Figure 1(a) presents a flowchart that intuitively illustrates the modules discussed in subsequent sections. Additionally, Figure 1(b) provides a visualization of the covariance matrices.

To study the energy imbalance across different levels of the network, we have tracked the total energy of each layer during training, along with the test and training loss, and compared it against that of BP. We have performed a broad study that tests multiple models, datasets, and setups, which we mostly report in the supplementary material, while presenting in Figure 2 the plots of the best performing models. As BP does not have a proper definition of energy, we have used the squared error of every layer computed during the backward pass, equivalent to the error of *PC* when it comes to the update of the weight parameters. As it can be observed, in PCNs there is a significant energy imbalance, where early layers have multiple orders of magnitude less energy than later layers. This does not happen in BP-trained models, that exhibit a more uniform energy distribution across layers, with even the layer of lowest energy above 10^{-2} . This set of experiments shows the potential reason why deep PC models do not perform well. Our proposed methods (second row) seem to slightly mitigate such an energy imbalance, despite it being still very significant. However, this partial mitigation is significant enough to allow the model to fit the training set. In the rest of the section, we describe the methods that we have used to address this major bottleneck.

Spiking Precision. Training predictive coding models involves a critical trade-off between stability and the efficient propagation of error signals. On the one hand, large learning rates α for the neural activities can lead to instabilities: most of the best results in the field have been obtained using a small learning rate, such as $\alpha = 0.05$ [Pinchetti et al., 2024]. On the other hand, such small learning rates can exponentially slow down the propagation of error signals across model layers, as noted in the supplementary material of [Song et al., 2020]. To this end, we propose to modulate the precision having a *spike* proportional to the learning rate the first time the energy — initially concentrated in the output neurons — reaches a specific layer. In terms of temporal scheduling, this happens at $l = L - t$. For a network with L layers and T inference steps, the proposed spiking precision hence is:

$$\Sigma_t^l = \begin{cases} \alpha & \text{when } l = L - t, \\ 1, & \text{otherwise.} \end{cases} \quad (4)$$

Intuitively, the spikes allow the energy to be well propagated from the last to the first layer during the first L iterations, with the other updates happening as usual. While this method has the additional advantage of not introducing any new hyperparameter, it fails to address the second problem that we highlighted: that the large energy and continuous updates make the neural activities diverge too much from the forward pass.

Decaying Precision. Building upon the idea of balancing stability and efficient error propagation, we introduce a decaying precision strategy. Here, the precision of different layers decays exponentially over time, as defined as follows:

$$\Sigma_t^l = \begin{cases} \frac{\sum_{j=0}^{T-L+l} e^{-k \cdot j}}{e^{-k \cdot (l-L+t)}}, & \text{when } l \geq L - t, \\ 1, & \text{when } l < L - t. \end{cases} \quad (5)$$

Here, the numerator sum serves as a normalization term that ensures that the sum of the layer-wise precisions over time is equal to one, that is, $\sum_{t=1}^T (\Sigma_t^l)^{-1} = 1$. The denominator $e^{-k \cdot (l-L+t)}$ allows lower layers to receive larger weights when activated ($l \geq L - t$), thereby helping to achieve a more balanced energy distribution during the inference phase, k is a hyperparameter that controls the strength of this balancing effect, the search range is presented in Table 5. It also ensures that each layer experiences a significant boost in precision precisely when the energy from the output first reaches that layer ($l = L - t$). When $l < L - t$, we set $\Sigma_t^l = 1$.

Forward Updates. Due to large prediction errors that we find in the last layers, the neural activities observed at the end of the inference process tend to significantly deviate from their initial feed-forward values. But the feedforward values are the ones that are then used for predictions. We then conjecture that synaptic weight updates based on \mathbf{x}_T^l could potentially introduce errors that accumulate with network depth, leading to performance degradation in deeper architectures. To assess whether the proposed conjecture is correct, we introduce a new method for updating the weight parameters that uses both the starting and final states of neurons, according to the energy function defined as

$$\tilde{E}_T = \frac{1}{2} \sum_l \frac{\|\tilde{\varepsilon}_T^l\|^2}{\Sigma_t^l}, \quad \text{where } \tilde{\varepsilon}_T^l = \mathbf{x}_T^l - \mu_0^l. \quad (6)$$

Our method makes sure that weight adjustments stay connected to the initial feed-forward predictions while incorporating the refined representations obtained through iterative inference. This approach has the advantage of maintaining stability during learning and prevents the accumulation of errors in deeper layers, which is crucial for scaling PC networks, but also the disadvantage of storing information in memory, which is then used for the weight update only, making it slightly less bioplausible than the original formulation. A similar energy function has been used in a different way in a previous work, where the authors used it to guide the update of the neural activities instead of the weight updates [Whittington and Bogacz, 2017]. The pseudocode is provided in Algorithm 1.

BatchNorm Freezing (BF). BatchNorm has proven instrumental in stabilizing the training of deep neural networks, as it mitigates gradient-related issues and ensures smooth gradient propagation. During training, it achieves this by normalizing layer activations through the function

$$\text{BN}(x) = \gamma \left(\frac{x - \mu_B}{\sqrt{\sigma_B^2 + \epsilon}} \right) + \beta, \quad (7)$$

where γ and β are learnable parameters, and μ_B and σ_B^2 are the mean and variance of the minibatch B . At test time, it uses statistics μ_r and σ_r^2 learned through exponential moving averages.

Algorithm 1 Learning a dataset $\mathcal{D} = \{\mathbf{o}_i, \mathbf{y}_i\}$ with forward updates

Require: \mathbf{x}_0^0 is fixed to \mathbf{o}_i and \mathbf{x}_t^L is fixed to \mathbf{y}_i for every mini-batch.

- 1: **for** $t = 1$ to T **do**
 - 2: **for** every level ℓ **do**
 - 3: Update \mathbf{x}_t^ℓ to minimize E_t .
 - 4: **end for**
 - 5: **if** $t = T$ **then**
 - 6: Update \mathbf{W}^l to minimize \tilde{E}_T .
 - 7: **end if**
 - 8: **end for**
-

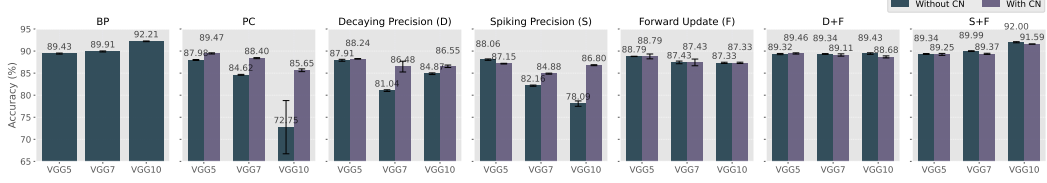


Figure 4: Test accuracies of different algorithms on the CIFAR10 dataset, tested on models of different depths. From left to right, we have first models trained with BP, second models trained with PC, while the rest represents combinations of the novel proposed in this work.

However, when applied directly to PCNs, BatchNorm fails to yield similar improvements. We hypothesize that this failure results from the iterative inference phase, where processing the same batch multiple times leads to a possible overfitting of the layer statistics. To address this issue, we propose BatchNorm Freezing (BF), a modification that freezes the states of the BatchNorm state during the inference phase, and updates running statistics exclusively during the learning phase while still using batch statistics for normalization during inference iterations. Our experimental results demonstrate that this modification not only preserves network convergence but also enhances performance, suggesting that its ability to stabilize activation distributions effectively supports the energy-based optimization in PC architectures.

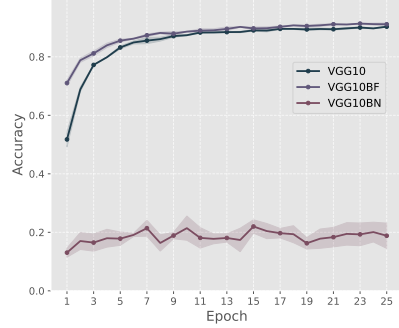


Figure 3: Test accuracy between models with the standard formulation of BN, without BN, and our proposed BF.

5 Experiments

In this section, we test our proposed methods combined on architectures with more than 7 layers, and show that we are able to reach performance comparable to those of BP when trained on models with the same complexity. To provide a comprehensive evaluation, we test them on CIFAR-10/100 [Krizhevsky et al., 2009]. We consider the following three baselines: standard PC (described in Section 3), PC with center nudging (PC-CN), the best performing algorithm according to previous studies [Pinchetti et al., 2024, Scellier et al., 2024], and standard BP.² As architectures, we use VGG-like models [Simonyan and Zisserman, 2014], which are deep convolutional models followed by feedforward layers. Similarly to the setups of the aforementioned works, in this work we only consider models with a single feedforward layer after the convolutional layers. This allows us to check whether our proposed methods still suffer from performance degradation when the depth of the model increases. In all cases, we perform a large number of hyperparameter searches, report the best test accuracy obtained with early stopping, averaged over 5 runs. All the details needed to reproduce the results can be found in the supplementary material.

²Here, we follow the standard PC literature, where performance are compared against BP, and differs from standard works in the Eqprop literature, that uses BPTT as a baseline.

Table 1: Test accuracies of the different algorithms on different datasets.

Dataset	Algorithm	VGG5	VGG7	VGG10	VGG5BF	VGG7BF	VGG10BF
CIFAR10	BP	89.43 \pm 0.12	89.91 \pm 0.12	92.21\pm0.08	90.01 \pm 0.15	91.32 \pm 0.14	92.68 \pm 0.10
	PC	87.98 \pm 0.11	84.62 \pm 0.10	72.75 \pm 6.03	87.77 \pm 0.14	80.62 \pm 0.14	76.22 \pm 0.43
	Decaying Precision (D)	87.91 \pm 0.22	81.14 \pm 0.19	84.87 \pm 0.19	88.55 \pm 0.09	80.00 \pm 0.10	81.68 \pm 0.18
	Spiking Precision (S)	88.06 \pm 0.16	82.16 \pm 0.14	78.09 \pm 0.61	88.53 \pm 0.07	86.51 \pm 0.21	83.17 \pm 0.07
	Forward Update (F)	88.79 \pm 0.04	87.43 \pm 0.30	87.33 \pm 0.14	87.34 \pm 0.13	85.91 \pm 0.09	79.43 \pm 0.20
	D+F	89.32 \pm 0.14	89.34 \pm 0.09	89.43 \pm 0.18	90.37\pm0.13	91.48\pm0.12	91.46 \pm 0.12
	S+F	89.45\pm0.18	90.08\pm0.21	92.07 \pm 0.10	89.30 \pm 0.13	90.89 \pm 0.04	93.27\pm0.10
CIFAR100 (Top-1)	BP	66.28 \pm 0.23	65.36 \pm 0.15	69.35\pm0.16	67.39 \pm 0.25	67.67 \pm 0.11	71.25 \pm 0.21
	PC	60.00 \pm 0.19	56.80 \pm 0.14	45.86 \pm 1.70	61.84 \pm 0.18	55.57 \pm 0.14	50.76 \pm 0.37
	Decaying Precision (D)	57.76 \pm 0.33	45.05 \pm 0.37	55.66 \pm 0.88	66.05 \pm 0.12	51.11 \pm 0.32	53.27 \pm 0.48
	Spiking Precision (S)	59.18 \pm 0.20	56.98 \pm 0.19	51.56 \pm 0.16	60.34 \pm 0.28	55.74 \pm 0.15	56.24 \pm 0.37
	Forward Update (F)	65.34 \pm 0.07	64.50 \pm 0.14	61.69 \pm 0.79	64.69 \pm 0.17	63.52 \pm 0.32	60.33 \pm 0.30
	D+F	66.10 \pm 0.09	64.86 \pm 0.10	66.54 \pm 0.12	67.56\pm0.25	67.27 \pm 0.21	69.81 \pm 0.22
	S+F	66.49\pm0.15	66.34\pm0.22	63.35 \pm 0.12	67.16 \pm 0.16	67.71\pm0.10	72.02\pm0.12
CIFAR100 (Top-5)	BP	85.85 \pm 0.27	84.41 \pm 0.26	88.74\pm0.08	89.56 \pm 0.08	90.05\pm0.13	92.10\pm0.12
	PC	84.97 \pm 0.19	83.00 \pm 0.09	74.61 \pm 1.08	86.53 \pm 0.15	82.07 \pm 0.35	78.68 \pm 0.27
	Decaying Precision (D)	81.59 \pm 0.13	74.00 \pm 0.30	83.13 \pm 0.74	88.82 \pm 0.07	78.93 \pm 0.29	81.16 \pm 0.36
	Spiking Precision (S)	84.58 \pm 0.12	83.61 \pm 0.15	78.62 \pm 0.15	85.86 \pm 0.10	82.64 \pm 0.14	83.44 \pm 0.21
	Forward Update (F)	85.48 \pm 0.08	84.05 \pm 0.07	76.73 \pm 0.92	88.05 \pm 0.16	87.45 \pm 0.24	83.33 \pm 0.19
	D+F	85.85 \pm 0.10	83.80 \pm 0.20	86.10 \pm 0.21	89.84\pm0.17	89.74 \pm 0.12	91.24 \pm 0.07
	S+F	86.36\pm0.11	84.53\pm0.15	86.84 \pm 0.07	89.57 \pm 0.09	89.62 \pm 0.18	92.10\pm0.10

Performance Degradation. In the first experiment, we test some of the proposed algorithms on VGG models with different depths, and report the bar plots of their test accuracies as a function of the number of layers in Figure 4. The plots show that both the original formulation of PC and the one that uses center nudging significantly drop in test accuracy when the depth of the model is increased. In contrast, our proposed methods combining precision and forward updates (D+F, S+F) demonstrate excellent performance, notably avoiding the significant accuracy degradation as model depth increases. Particularly, spiking precision with forward updates is the only combination of methods that exhibits performance comparable to BP across VGG5/7/10 models. We will later see that this result will be consistent with the more complex experiments, where this method is still the one achieving the best performance overall. In models without forward update, consistent with previous findings, using center nudging enhances algorithm accuracy, with more pronounced effects as the number of model layers increases in most cases. However, we found that once forward update is added, center nudging ceases to yield performance benefits. To this end, from now on we will only report experiments that use the standard formulation of PC, without any nudging.

Test Accuracies. To better test the performance of our methods, as well as all the combinations and ablation studies, we report a comprehensive comparison in Table 1. The results show that for shallow networks, we can either match or approximate the performance of BP with all the methods. In deeper models, this is not the case, as we observe that standard PC performs badly, decaying precisions and spiking precisions slightly better, while forward updates well mitigate the degradation of performance. It is however the combination of both inference and update methods that performs the best, with spiking precisions and forward updates always slightly matching the performance of models trained with BP. To conclude, we note that batch freezing further improves the results, clearly showing that the best combination of methods is batch freezing, forward updates, and spiking precisions, which get the best results on all benchmarks when testing on a VGG10. In this case, we use models with normal BN when testing with BP.

Scaling up. To see how much our methods scale on larger datasets and deeper networks, we have also tested them on a VGG15 on the Tiny ImageNet [Le and Yang, 2015], a scaled down version of ImageNet with 200 classes. The model that we use is identical to the one proposed in the hybrid equilibrium propagation work [Nest and Ernoult, 2024]. The results, reported in Table 2, show even more strongly the effectiveness of our method with respect to the original formulation of PC. More in detail, we observe that most of the inference methods alone, even the ones that use precision weighting, fail to reach the performance of BP on this challenging task. However, the results are matched when we use in combination all of the novel methods presented in this work: forward updates, spiking precisions, and BatchNorm freezing.

Table 2: Test accuracies of the different algorithms on Tiny ImageNet.

Algorithm	Top-1 Accuracy		Top-5 Accuracy	
	VGG15	VGG15BF	VGG15	VGG15BF
BP	44.52\pm0.16	53.21\pm0.39	69.28\pm0.06	77.26\pm0.17
S+F	42.51 \pm 0.18	53.04 \pm 0.36	66.22 \pm 0.18	76.64 \pm 0.23
PC	22.95 \pm 1.50	22.91 \pm 0.61	47.04 \pm 2.04	45.64 \pm 0.63
Decaying Precision (D)	27.29 \pm 0.24	22.05 \pm 0.16	54.18 \pm 0.37	45.22 \pm 0.23
Spiking Precision (S)	18.36 \pm 0.36	17.95 \pm 0.14	39.24 \pm 0.31	39.87 \pm 0.51
Forward Update (F)	31.61 \pm 0.73	28.64 \pm 0.11	55.99 \pm 0.49	53.72 \pm 0.31
D+F	21.95 \pm 0.20	30.83 \pm 0.77	45.15 \pm 0.23	56.06 \pm 0.85

6 Conclusion

In this work, we have tackled the problem of scaling up predictive coding for image classification tasks. Specifically, we investigated the following research question: Why do deep models trained with the predictive coding energy fail to match the accuracy of their counterparts trained with backpropagation? We have addressed this by proposing two novel regularization techniques and showed that the combination of our approaches allows the training of deep predictive coding models that come close to the performance of backprop-based models on the same task on deep models. More in detail, we have trained a model with 15 hidden layers on Tiny Imagenet, a result previously obtained only by using hybrid models that have layers trained with both BP and EP. We believe that these results will inspire future work directed towards making this class of models work at scale, that will tackle more complex datasets and modalities that we have considered, such as the training of equilibrium propagation-based ResNets on ImageNet [He et al., 2016], or small transformer models.

Despite being a good starting point towards the scaling up of the performance of predictive coding and equilibrium propagation models, this work still has some limitations that will be addressed and better studied in future works. The first one relates to the derivation of a better understanding of the phenomenon of the energy imbalance, still not well studied: what causes it, and the correlation it has with the performance of the model on the test and train accuracy. This would allow us to scale to even larger datasets and benchmarks. A second limitation of the work is the presence of the value of the predictions at initialization during the forward updates, which means that the algorithm has to store this value in memory, adding a degree of biological implausibility. This sheds some light on another problem of this class of models, still caused by the energy imbalance: in later layers of the network, the predictions at convergence tend to diverge too much from the predictions at initialization, causing the consequent weight update to be suboptimal. Future work will investigate all of this, and use the derived knowledge to further improve the performance of this class of models, with a nice starting point being a contemporaneous study that theoretically shows it could be possible to train very deep feedforward models Innocenti et al. [2025]. Another contemporary work has tackled the same problem as ours by introducing sequential updates for the value nodes Goemaere et al. [2025], similar to a previously introduced variation of PC, that studied the equivalence between PC and backprop Song et al. [2020], Salvatori et al. [2022b].

Acknowledgments

This research was funded in part by the AXA Research Fund and in part by the Austrian Science Fund (FWF) 10.55776/COE12, and in part by VERSES AI. For open access purposes, the author has applied a CC BY public copyright license to any author accepted manuscript version arising from this submission.

References

- Yoshua Bengio. How auto-encoders could provide credit assignment in deep networks via target propagation. *arXiv:1407.7906*, 2014.
- Andy Clark. The many faces of precision (replies to commentaries on “whatever next? neural prediction, situated agents, and the future of cognitive science”). *Frontiers in Psychology*, 4:270, 2013.
- Maxence Ernout, Rasmus Højer, and Jack Kendall. A cookbook for hardware-friendly implicit learning on static data. In *NeurIPS 2024 Workshop Machine Learning with new Compute Paradigms*.
- Karl Friston. A theory of cortical responses. *Philosophical Transactions of the Royal Society B: Biological Sciences*, 360(1456), 2005.
- Karl Friston and Stefan Kiebel. Predictive coding under the free-energy principle. *Philosophical transactions of the Royal Society B: Biological Sciences*, 364(1521):1211–1221, 2009.
- Cédric Goemaere, Gaspard Oliviers, Rafal Bogacz, and Thomas Demeester. Error optimization: Overcoming exponential signal decay in deep predictive coding networks. *arXiv preprint arXiv:2505.20137*, 2025.
- Wilfried Haensch, Tayfun Gokmen, and Ruchir Puri. The next generation of deep learning hardware: Analog computing. *Proceedings of the IEEE*, 107(1):108–122, 2018.
- Kaiming He, Xiangyu Zhang, Shaoqing Ren, and Jian Sun. Deep residual learning for image recognition. In *Proceedings of the IEEE Conference on Computer Vision and Pattern Recognition*, 2016.
- Geoffrey Hinton. The forward-forward algorithm: Some preliminary investigations. *arXiv preprint arXiv:2212.13345*, 2022.
- Sepp Hochreiter. The vanishing gradient problem during learning recurrent neural nets and problem solutions. *International Journal of Uncertainty, Fuzziness and Knowledge-Based Systems*, 6(02): 107–116, 1998.
- J J Hopfield. Neural networks and physical systems with emergent collective computational abilities. *Proceedings of the National Academy of Sciences*, 79, 1982.
- Francesco Innocenti, El Mehdi Achour, and Christopher L Buckley. μ PC: Scaling predictive coding to 100+ layer networks. *arXiv preprint arXiv:2505.13124*, 2025.
- Sergey Ioffe and Christian Szegedy. Batch normalization: Accelerating deep network training by reducing internal covariate shift. In *International Conference on Machine Learning*, pages 448–456. PMLR, 2015.
- Jack Kendall, Ross Pantone, Kalpana Manickavasagam, Yoshua Bengio, and Benjamin Scellier. Training end-to-end analog neural networks with equilibrium propagation. *arXiv preprint arXiv:2006.01981*, 2020.
- Alex Krizhevsky, Geoffrey Hinton, et al. Learning multiple layers of features from tiny images. 2009.
- Dmitry Krotov and John J. Hopfield. Dense associative memory for pattern recognition. In *Advances in Neural Information Processing Systems*, 2016.
- Axel Laborieux and Friedemann Zenke. Holomorphic equilibrium propagation computes exact gradients through finite size oscillations. *Advances in Neural Information Processing Systems*, 35: 12950–12963, 2022.
- Axel Laborieux, Maxence Ernout, Benjamin Scellier, Yoshua Bengio, Julie Grollier, and Damien Querlioz. Scaling equilibrium propagation to deep convnets by drastically reducing its gradient estimator bias. *Frontiers in Neuroscience*, 15:129, 2021.
- Ya Le and Xuan Yang. Tiny imagenet visual recognition challenge. *CS 231N*, 7(7):3, 2015.

- Ali Momeni, Babak Rahmani, Benjamin Scellier, Logan G. Wright, Peter L. McMahon, Clara C Wanjura, Yuhang Li, Anas Skalli, Natalia G Berloff, Tatsuhiro Onodera, et al. Training of physical neural networks. *arXiv preprint arXiv:2406.03372*, 2024.
- Javier R. Movellan. Contrastive Hebbian learning in the continuous hopfield model. In *Connectionist Models*, pages 10–17. Elsevier, 1991.
- David Mumford. On the computational architecture of the neocortex. *Biological Cybernetics*, 66(3): 241–251, 1992.
- Timothy Nest and Maxence Ernoult. Towards training digitally-tied analog blocks via hybrid gradient computation. *Advances in Neural Information Processing Systems*, 37:83877–83914, 2024.
- Andre Ofner, Raihan Kabir Ratul, Suhita Ghosh, and Sebastian Stober. Predictive coding, precision and natural gradients. *arXiv preprint arXiv:2111.06942*, 2021.
- Alex Ororbia and Daniel Kifer. The neural coding framework for learning generative models. *arXiv:2012.03405*, 2020.
- Luca Pinchetti, Tommaso Salvatori, Beren Millidge, Yuhang Song, Yordan Yordanov, and Thomas Lukasiewicz. Predictive coding beyond Gaussian distributions. *36th Conference on Neural Information Processing Systems*, 2022.
- Luca Pinchetti, Chang Qi, Oleh Lokshyn, Gaspard Olivers, Cornelius Emde, Mufeng Tang, Amine M’Charrak, Simon Frieder, Bayar Menzat, Rafal Bogacz, et al. Benchmarking predictive coding networks—made simple. *arXiv preprint arXiv:2407.01163*, 2024.
- Rajesh P. N. Rao and Dana H. Ballard. Predictive coding in the visual cortex: A functional interpretation of some extra-classical receptive-field effects. *Nature Neuroscience*, 2(1):79–87, 1999.
- David E. Rumelhart, Geoffrey E. Hinton, and Ronald J. Williams. Learning representations by back-propagating errors. *Nature*, 323(6088):533–536, 1986.
- Tommaso Salvatori, Yuhang Song, Yujian Hong, Lei Sha, Simon Frieder, Zhenghua Xu, Rafal Bogacz, and Thomas Lukasiewicz. Associative memories via predictive coding. In *Advances in Neural Information Processing Systems*, volume 34, 2021.
- Tommaso Salvatori, Yuhang Song, Thomas Lukasiewicz, Rafal Bogacz, and Zhenghua Xu. Reverse differentiation via predictive coding. In *Proc. AAAI*, 2022a.
- Tommaso Salvatori, Yuhang Song, Zhenghua Xu, Thomas Lukasiewicz, and Rafal Bogacz. Reverse differentiation via predictive coding. In *Proceedings of the 36th AAAI Conference on Artificial Intelligence*. AAAI Press, 2022b.
- Tommaso Salvatori, Ankur Mali, Christopher L Buckley, Thomas Lukasiewicz, Rajesh PN Rao, Karl Friston, and Alexander Ororbia. Brain-inspired computational intelligence via predictive coding. *arXiv preprint arXiv:2308.07870*, 2023.
- Benjamin Scellier. Quantum equilibrium propagation: Gradient-descent training of quantum systems. *arXiv preprint arXiv:2406.00879*, 2024.
- Benjamin Scellier and Yoshua Bengio. Equilibrium propagation: Bridging the gap between energy-based models and backpropagation. *Frontiers in Computational Neuroscience*, 11:24, 2017.
- Benjamin Scellier, Siddhartha Mishra, Yoshua Bengio, and Yann Ollivier. Agnostic physics-driven deep learning. *arXiv preprint arXiv:2205.15021*, 2022.
- Benjamin Scellier, Maxence Ernoult, Jack Kendall, and Suhas Kumar. Energy-based learning algorithms for analog computing: a comparative study. *Advances in Neural Information Processing Systems*, 36, 2024.
- Eli Sennesh, Hao Wu, and Tommaso Salvatori. Divide-and-conquer predictive coding: a structured bayesian inference algorithm. *arXiv preprint arXiv:2408.05834*, 2024.

- Karen Simonyan and Andrew Zisserman. Very deep convolutional networks for large-scale image recognition. *arXiv preprint arXiv:1409.1556*, 2014.
- Yuhang Song, Thomas Lukasiewicz, Zhenghua Xu, and Rafal Bogacz. Can the brain do backpropagation? — Exact implementation of backpropagation in predictive coding networks. In *Advances in Neural Information Processing Systems*, volume 33, 2020.
- Hsinyu Tsai, Stefano Ambrogio, Pritish Narayanan, Robert M. Shelby, and Geoffrey W. Burr. Recent progress in analog memory-based accelerators for deep learning. *Journal of Physics D: Applied Physics*, 51(28):283001, 2018.
- Shuhei Watanabe. Tree-structured parzen estimator: Understanding its algorithm components and their roles for better empirical performance. *arXiv preprint arXiv:2304.11127*, 2023.
- James C. R. Whittington and Rafal Bogacz. An approximation of the error backpropagation algorithm in a predictive coding network with local Hebbian synaptic plasticity. *Neural Computation*, 29(5), 2017.
- Logan G. Wright, Tatsuhiko Onodera, Martin M. Stein, Tianyu Wang, Darren T. Schachter, Zoey Hu, and Peter L. McMahon. Deep physical neural networks trained with backpropagation. *Nature*, 601(7894):549–555, 2022.
- Nicolas Zucchet and João Sacramento. Beyond backpropagation: bilevel optimization through implicit differentiation and equilibrium propagation. *Neural Computation*, 34(12):2309–2346, 2022.

Appendix

Here we provide an explanation of the performed experiments, as well as a detailed description of all the parameters needed to replicate the results of the paper. We also provide an ablation study that shows the performance of the individual methods in isolation.

A Experiments Setting

Model. We conducted experiments on four models: VGG5, VGG7, VGG10, and VGG15. The detailed architectures of these models are presented in Table 3.

Table 3: Detailed architectures of base models

	VGG5	VGG7
Channel Sizes	[128, 256, 512, 512]	[128, 128, 256, 256, 512, 512]
Kernel Sizes	[3, 3, 3, 3]	[3, 3, 3, 3, 3, 3]
Strides	[1, 1, 1, 1]	[1, 1, 1, 1, 1, 1]
Paddings	[1, 1, 1, 0]	[1, 1, 1, 0, 1, 0]
Pool window	2×2	2×2
Pool stride	2	2
Linear Layers	1	1

	VGG10	VGG15
Channel Sizes	[64, [128]x3, [256]x4, 512]	[64, 64, 128, 128, [256]x3, [512]x6]
Kernel Sizes	[3, 3, 3, 3, 3, 3, 3, 3]	[3, 3, 3, 3, 3, 3, 3, 3, 3, 3, 3, 3]
Strides	[1, 1, 1, 1, 1, 1, 1, 1]	[1, 1, 1, 1, 1, 1, 1, 1, 1, 1, 1, 1]
Paddings	[1, 1, 1, 1, 1, 1, 1, 1]	[1, 1, 1, 1, 1, 1, 1, 1, 1, 1, 1, 1]
Pool window	2×2	2×2
Pool stride	2	2
Linear Layers	1	2

Experiments. The benchmark results of above models are obtained with CIFAR10, CIFAR100 and Tiny ImageNet. The datasets are normalized as in Table 4.

Table 4: Data normalization

	Mean (μ)	Std (σ)
CIFAR10	[0.4914, 0.4822, 0.4465]	[0.2023, 0.1994, 0.2010]
CIFAR100	[0.5071, 0.4867, 0.4408]	[0.2675, 0.2565, 0.2761]
Tiny ImageNet	[0.485, 0.456, 0.406]	[0.229, 0.224, 0.225]

For data augmentation on CIFAR10, CIFAR100, and Tiny ImageNet training sets, we use 50% random horizontal flipping. We also apply random cropping with different setups. For CIFAR10 and CIFAR100, images are randomly cropped to 32x32 resolution with 4-pixel padding. For Tiny ImageNet, images are randomly cropped to 64x64 resolution images with 8-pixel padding. For testing on those datasets, we applied only standard data normalization, without using any additional data augmentation techniques.

For the optimizer and scheduler, we employ mini-batch stochastic gradient descent (SGD) with momentum for updating x during the relaxation phase. In the Spiking Decaying approach, the learning rate for the last hidden node x decays exponentially with iteration t according to $lr = lr_x^t$. While we evaluated this exponential decay strategy across other methods, it yielded no performance improvements, leading us to exclude it from their final implementations. For the learning phase, we optimize weights W using AdamW with weight decay. The learning rate schedule follows a warmup-cosine annealing pattern without restarts. This scheduler initiates training with a low learning rate during the warmup period, then smoothly transitions to a cosine-shaped decay curve, preventing abrupt performance degradation. The schedule parameters are configured as follows: the peak learning rate reaches 1.1 times the initial rate, the final learning rate settles at 0.1 times the initial rate, and the warmup phase spans 10% of the total iteration steps.

Table 5: Hyperparameters search configuration

Parameter	PCNs	BP
Epoch	25	
Batch Size	128	
Activation	[leaky relu, gelu, hard tanh, relu]	
k	[1.0, 1.5, 2.0]	-
β	[0.0, 1.0], 0.15 ¹	-
lr_x^*	(5e-3, 9e-1) ²	-
lr_w	(1e-5, 3e-2) ²	(1e-5, 3e-4) ²
$momentum_x$	[0.0, 1.0], 0.1 ¹	-
$weightdecay_w$	(1e-5, 1e-2) ²	
T (VGG-5)	[5, 6, 7, 8]	-
T (VGG-7)	[7, 9, 11, 13]	-
T (VGG-10)	[10, 12, 14, 16]	-
T (VGG-15)	[15, 17, 19, 21]	-

¹: “[a, b], c” denotes a sequence of values from a to b with a step size of c.

²: “(a, b)” represents a log-uniform distribution between a and b.

Table 6: Comparison of the training times (seconds) of BP against PCNs on different architectures and datasets.

	BP	PC	S + F
VGG-5 - CIFAR10 (T = 5)	1.16 \pm 0.02	2.59 \pm 0.01	2.37 \pm 0.01
VGG-7 - CIFAR10 (T = 7)	1.29 \pm 0.02	3.75 \pm 0.01	3.58 \pm 0.01
VGG-10 - CIFAR100 (T = 10)	2.03 \pm 0.06	10.38 \pm 0.01	10.88 \pm 0.02
VGG-15 - TinyImageNet (T = 15)	9.40 \pm 0.07	79.61 \pm 0.08	77.58 \pm 0.02

We conduct hyperparameter selection based on the search space specified in Table 5. All experiments were implemented using the PCX library Pinchetti et al. [2024], a JAX-based framework specifically designed for predictive coding networks that provides comprehensive benchmarking capabilities. All the experiments were conducted on NVIDIA A100/H100 GPUs, with each trial involving a hyperparameter search using the Tree-Structured Parzen Estimator (TPE) algorithm Watanabe [2023] over 500 iterations. The results presented in Table 1 and Figure 4 are obtained using 5 different random seeds (selected from 0-4) with the optimal hyperparameter configuration. The training process is capped at 50 epochs, with an early stopping mechanism that terminates training if no accuracy improvement is observed for 10 consecutive epochs. To maintain consistency with the hyperparameter search settings, we employ a two-phase learning rate schedule: during the first 25 epochs, the weight learning rate follows a warmup-cosine-annealing schedule as previously described, after which it remains fixed at the final learning rate of the scheduler. For the results shown in Figure 2 and 5, we utilize a single random seed with the optimal hyperparameters, setting the maximum training epochs to 50 without implementing early stopping. The weight learning rate schedule remains identical to the aforementioned approach.

A.1 Computational Complexity

In Table 6, we present the average time required to train one epoch using *BP*, *PC*, and Spiking Precision + Forward Update (*S + F*) across various tasks on a single H100 GPU. To eliminate the overhead associated with loading datasets into memory, we began timing from the fifth epoch onward, calculating the average duration across five consecutive epochs. We repeated this measurement process five times and report the mean and standard deviation of these five experimental runs. It is worth noting that the reported times for predictive coding suffer from an implementation bottleneck: despite the possibility of updating all the neural activities in parallel, our library does not allow that. This largely slows down our models when trained on deep architectures.

Results. From the table, we observe that *PC* and our proposed *S + F* method have comparable training times, but both are slower than *BP*, with this ratio increasing as the number of model layers

increases, mostly for the bottleneck just described. During the forward pass, BP and $PCNs$ (PC , $S + F$) perform identical computations, resulting in equivalent computational complexity. However, during the backward pass, $PCNs$ require updating the neuronal activations x before updating weights W , with x needing T iterations of updates. The fact that the optimal value of T is always equal to or slightly larger than the number of layers further explains why $PCNs$ are slower compared to BP when the model depth increases, despite this not being as much of a bottleneck as the full parallelization of the operations.

B Energy Propagation in models

In this section, we deliberately selected the VGG5 and VGG7 architectures from our experimental framework for comparative energy distribution visualization. Figure 5 and Figure 2 present layer-wise energy distribution and classification accuracy among Backpropagation (BP), Predictive Coding (PC), our proposed Decaying Precision + Forward Update ($D + F$), and our proposed Spiking Precision + Forward Update ($S + F$) evaluated on VGG5 (Figure 5(a)), VGG7 (Figure 5(b)) and VGG10 (Figure 2) architectures using the CIFAR10 dataset.

In VGG5, while all four methods demonstrate comparable accuracy, our proposed methods achieve superior energy equilibrium across network layers compared to PC , thereby demonstrating their effectiveness in enhancing the model’s layer-wise energy balance. Interestingly, $PCNs$ achieves good results despite having a less uniform energy distribution than BP . Compared to energy propagation in VGG5, Figure 5(b) and Figure 2 reveal a significant energy imbalance in the standard PC when implemented in VGG7/10 architectures, which correlates with degraded test accuracy. In contrast, our proposed method maintains superior energy balance compared to standard PC in deep networks while achieving comparable—or even superior—test accuracy relative to BP .

C Ablation Study

In this section, we conducted ablation studies to evaluate the effectiveness of each proposed component. These experiments allowed us to quantify the individual contribution of each component and their synergistic effects when combined. The results are presented in Table 1.

Firstly, we observe that removing forward updates (using the standard PC model with decaying/spiking Precision) causes significant accuracy degradation, which becomes more pronounced with increasing network depth. Simultaneously, the effectiveness of center nudging reappears when forward updates are removed, with its impact also strengthening in deeper networks as shown in Figure 4. This phenomenon confirms our earlier hypothesis: synaptic weight updates based on x_t^l may introduce errors that accumulate across layers, leading to performance degradation in deep architectures.

Secondly, we observed that removing the decaying/spiking precision module leads to performance degradation in most cases. This effect is evident in deep models such as VGG7/10, where the energy distribution across layers becomes significantly imbalanced without the precision term. As shown in Figure 6 and Figure 5, in the VGG7 architecture with spiking precision and forward update, the first layer’s energy proportion is approximately 10^{-6} , whereas in the model without spiking precision, this proportion drops dramatically to 10^{-12} . Visualization of layer-wise energy distributions between decaying/spiking precision + forward update versus only forward update confirms that our proposed precision methods successfully balance energy distribution across layers, which contributes to improved model performance.

Thirdly, we found that BatchNorm Freezing (BF) significantly enhances model performance when combined with our precision module and forward update mechanism. As illustrated in Figure 7, the integration of BF with our proposed methods ($D + F$ and $S + F$) consistently improved accuracy across all model depths and both CIFAR10 and CIFAR100 datasets. Specifically, the $S + F$ configuration with BF achieved peak performance of 93.27% on CIFAR10 and 72.02% on CIFAR100 with the VGG10 architecture, outperforming even the BP baseline. In contrast, when BF was applied to standard PC or only with forward Update, we observed performance degradation rather than improvement in most cases. For models using only decaying precision or spiking precision without forward update, the effect of BF was inconsistent and unpredictable across different network depths. These results suggest that the synergy between our proposed components is crucial— BF

appears to stabilize the training dynamics specifically when used in conjunction with both our energy balancing mechanisms (either decaying or spiking precision) and forward update. This interaction allows deeper networks to maintain stable gradients throughout the training process, resulting in more robust optimization and ultimately higher classification accuracy.

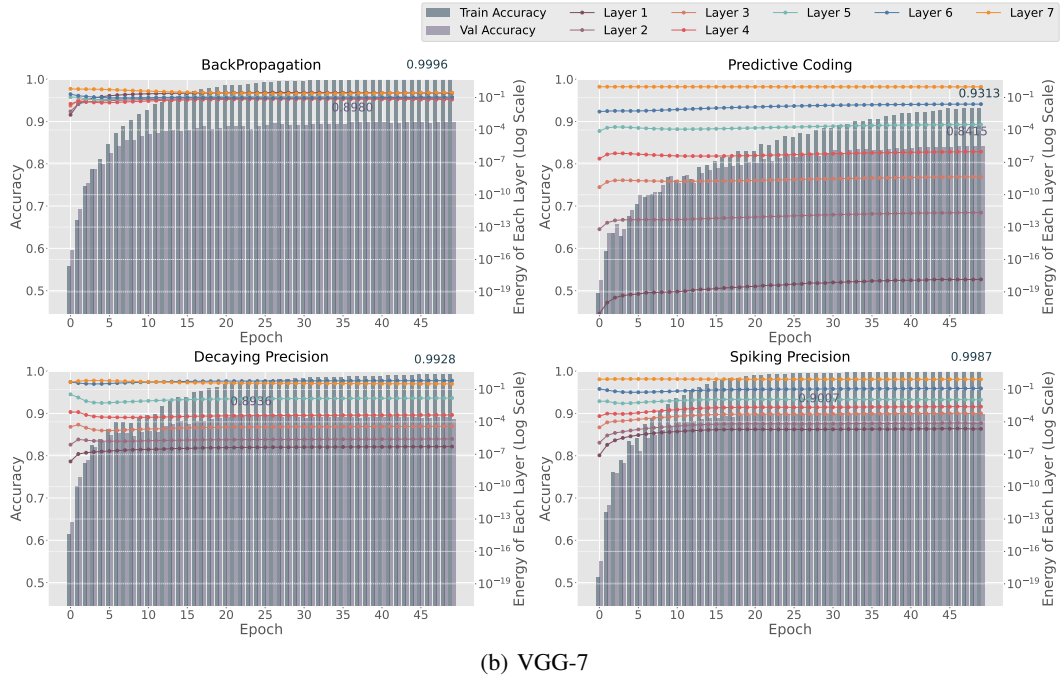
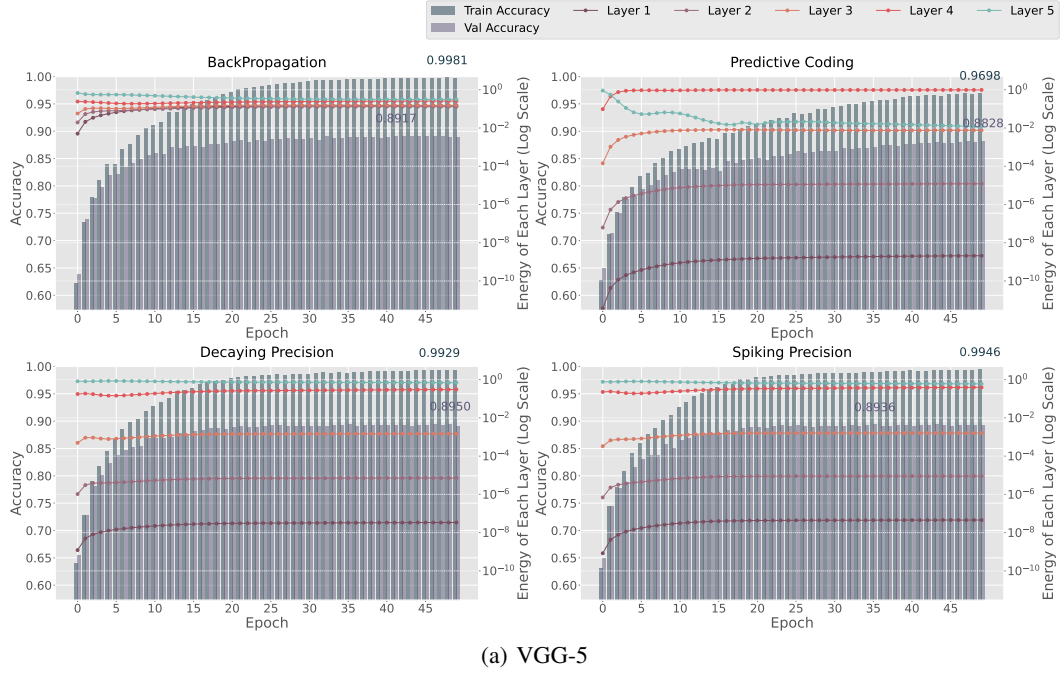


Figure 5: Layer-wise Energy Distribution and Accuracy Comparison between BP, PC and Decaying Precision/Spiking Precision with Forward Update in VGG5(a) and VGG7(b) on the CIFAR10 dataset. The colored lines represent the total energy of the individual layers of the model (or, the squared error of every layer for BP). The vertical lines represent the train and test accuracies of the model.

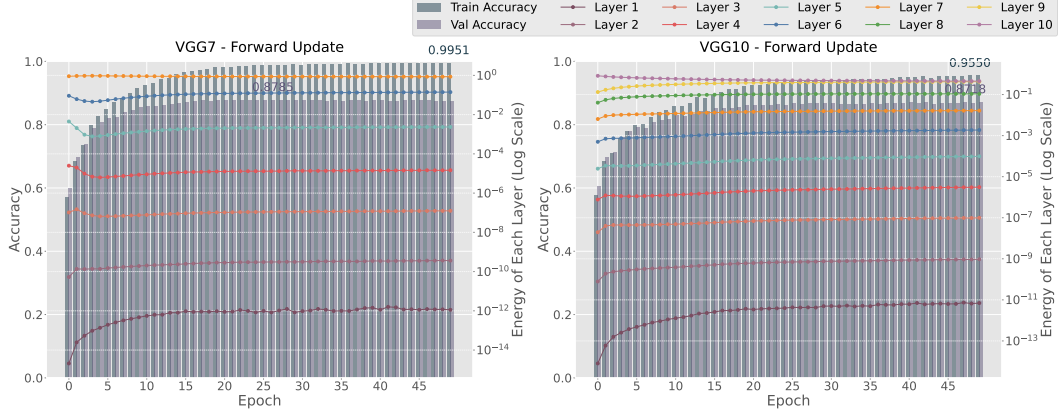


Figure 6: Layer-wise Energy Distribution and Accuracy of Forward Update in VGG7 and VGG10 on the CIFAR10 dataset. The colored lines represent the total energy of the individual layers of the model. The vertical lines represent the train and test accuracies of the model.

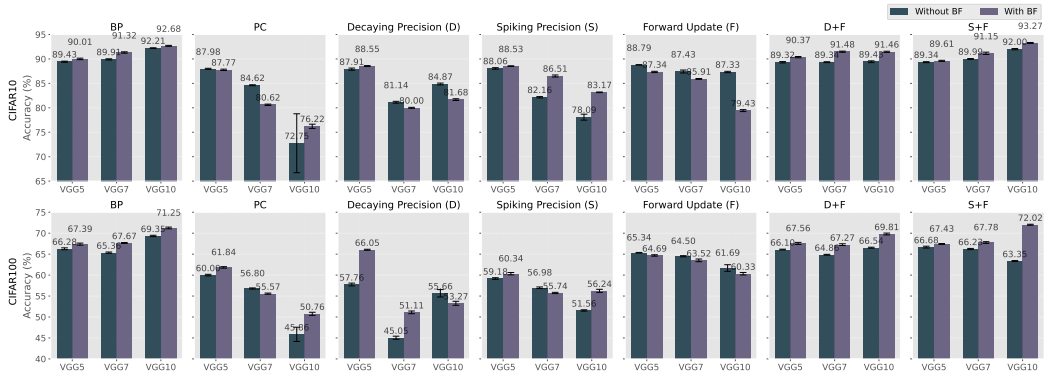


Figure 7: Test accuracies of different algorithms on the CIFAR10/100 datasets across models of varying depths, comparing different methods with and without BatchNorm freezing.